RSC Advances

This article can be cited before page numbers have been issued, to do this please use: P. Gangadharan, I. Nambi, S. Jaganathan and P. Veeramani, *RSC Adv.*, 2016, DOI: 10.1039/C6RA13911F.

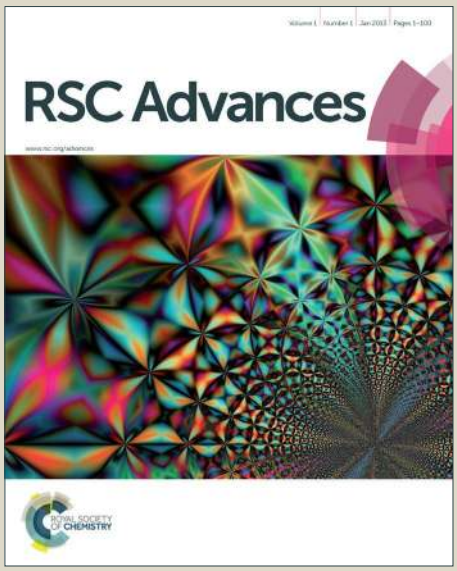

ROYAL SOCIETY OF CHEMISTRY

www.rsc.org/advances

View Article Online
DOI: 10.1039/C6RA13911F

Journal Name

ARTICLE

Heterocyclic aminopyrazine-reduced graphene oxide coated carbon cloth electrode as an active bio-electrocatalyst for extracellular electron transfer in microbial fuel cell

Received 00th January 20xx,
Accepted 00th January 20xx

DOI: 10.1039/x0xx00000x

www.rsc.org/RSC Advances

Praveena Gangadharan,‡[a] Indumathi M Nambi,[a]* Jaganathan Senthilnathan ‡[a] and Pavithra V M‡[a]

In the present study, a low molecular heterocyclic aminopyrazine (Apy) - reduced graphene oxide (r-GO) hybrid coated carbon cloth (r-GO-Apy-CC) was employed as an active and stable bio-electro catalyst in microbial fuel cell (MFC). The presence of imine (-NH-) and pyridinic (-N=C-) functional groups on r-GO-Apy-CC electrode plays a critical role in the formation of bacterial colonization and enhanced extracellular electron transfer (EET) over a considerable period. The bacterial colonization over r-GO-Apy-CC electrode was investigated in a Sacrificial Electrode Mode Reactor (SEMR) in which attached bacterial density with extracellular polysaccharides was monitored over a period. Simultaneously, a cyclic voltammetry (CV) was performed in Bioelectrochemical System (BES) reactor, resulted in an increased current density-voltage response from 0.27 mA cm^{-2} to 1.84 mA cm^{-2} over a period of time. In addition, when r-GO-Apy-CC was employed as an anode in MFC, the power density was nearly two times (1253 mW m^{-2}) than that of the MFC employed with plain carbon cloth (PCC) (663.7 mW m^{-2}) at a steady state condition. It was proposed that the combined effect of Apy hybridized with nanostructured r-GO provides large surface area for bacterial colonization. Moreover, the high bioelectrocatalytic activity was attributed to the low molecular nature of the Apy, which incorporated well into the EET pathway of the exoelectrogens by redox mechanism.

Introduction

In recent years, there have been a lot of studies devoted to obtaining an efficient anode material in microbial fuel cells (MFCs), as the interaction between anodes and microbes are the key role for electricity generation.[1–3] In MFCs, the electrochemically active microorganisms utilize extracellular electron transfer (EET) mechanisms such as outer membrane proteins, diffusion of soluble electron shuttles and extracellular biofilm matrix to transfer the electrons to the anode.[4–6] Ineffective microbe anode interaction results in poor charge transfer efficiency and low power densities, which limited MFCs for most of the envisioned applications.[7,8] Carbon-based electrodes such as graphite, carbon cloth (CC), carbon paper and carbon brush are commonly used as anodes in MFCs.[9,10] However, their applications are limited due to poor conductivity and low specific surface area for bacterial colonization.[11] Conversely, the conductivity and surface area of conventional carbon-based electrodes can be enhanced either by surface modification with nanostructured material or by making functionalized composite with other material, such as conductive polymers.[12,13]

Recently, researchers have found potential in nanostructured material such as single-/multi-walled carbon nanotubes,[14,15] carbon nanofibers[16] and nanostructured carbon-based nano-metal hybrids[17] for replacing or modifying conventional electrodes.[18] Among these, graphene gained enormous attention due to its outstanding properties such as high mechanical strength, high thermal conductivity and large specific surface area (2630 m^2 g^{-1}).[19–22] Numerous studies have reported that graphene-modified electrodes enhanced the performance of the anode by improving the EET mechanism through sp^2 hybridized carbon.[23,24] Moreover, its high specific surface area provides sufficient active sites for bacterial colonization, which effectively inject electron to the anode and this leads to an increase in current density.[25,26] The negative aspect of graphene is that it shows poor dispersibility in most of the solvents due to the strong van der Waals force of attraction between each of the layer.[27] Graphene oxide (GO) or reduced graphene oxide (r-GO) shows very high dispersibility in most of the solvents. However, GO displays poor electrical properties due to the presence of sp^3 carbon, which hinders the electron mobility and limits its electrode and sensor applications.[20,28]

[a] *Environmental and Water Resources Engineering Division, Department of Civil Engineering. Indian Institute of Technology, Madras -600036, India.*
*Corresponding Author. E-mail:-indunambi@iitm.ac.in. Tel:- +91 - 44 – 22574289. Fax: - +91-44-22574252.
†Electronic Supplementary Information (ESI) available: See DOI: 10.1039/x0xx00000x
‡ All authors equally contributed to this work

View Article Online
DOI: 10.1039/C6RA13911F

Many researchers have been extensively studied the surface modification of GO/r-GO with organic moieties like polyaniline, porphyrin, poly (o-phenylenediamine), ionic liquid, polythiophene and polypyrrole.[29–34] The high molecular organic moieties form a hybrid through either chemisorption or covalent or noncovalent or a combination of both (σ–σ, σ–π and π–π) interactions with oxygen functional groups of GO/r-GO.[35] Nevertheless, most of these organic moieties have high molecular weight (> 15,000 g mole^{-1}) and are made up of lengthy carbon chains with various functional groups. In addition, stability, chemical and electrical properties of GO/r-GO hybrids, which are prepared by the use of high molecular organic moieties, do not remain the same after one or two cycles. Hence, the long-term stability and electrical properties of high molecular organic moieties GO/r-GO hybrids have to be explored further.[17] However, finding new organic moieties with low molecular weight is highly challenging as it requires good biocompatibility, noble environmental stability and should be non-toxic to microorganisms.[36] Furthermore, it should act as a conductive bridge with superior electrical conductivity to facilitate efficient electron transfer between microbes and electrodes by reducing the activation energy barrier at the electrode interface.[3] Earlier, Darwish *et al.*[37] studied the electrical conductivity of low molecular aminopyrazine organic moieties, and reported higher electrical conductivity due to increased π electron delocalization in the charge transfer complexes. Therefore, an effort was made to incorporate low molecular aminopyrazine (Apy) organic moieties (95.10 g mole^{-1}) unified with r-GO as an electrode material for biofilm formation as well as for power generation. The unification of Apy into r-GO is expected to increase the dispersibility of r-GO in solvents and improve the electrical conductivity of the electrode material for higher power generation.

In this study, partially reduced GO aminopyrazine (r-GO-Apy) hybrid is developed and its feasibility as an electrode material in the anodic chamber was explored with a two-chambered MFC. A highly active r-GO-Apy hybrid was fabricated by coating on a commercial plain carbon cloth (PCC) by a simple "brush coating and drying" process. The performance of the newly synthesized material was evaluated by the following experiments. (i) Sacrificial Electrode Mode Reactor (SEMR) was accustomed to study the biocompatibility of the newly fabricated r-GO-Apy-CC by analysing each electrode periodically as a sacrificial method. (ii) Bioelectrochemical System (BES) was employed to study the electrocatalytic activity of r-GO-Apy-CC. (iii) MFC was used to understand the response of electrochemically active microorganisms over r-GO-Apy-CC electrode for power production.

Results and discussion

Chemical and electrical properties of r-GO-Apy hybrid material

UV-Vis spectrum of GO (Fig. 1a) shows the intense band at 229 nm (π–π) along with a weak band at 292 nm. For r-GO, the GO band appeared at 229 nm is shifted to 277 nm (n- π) which clearly indicates the reduction of GO into r-GO (Fig. 1a).[28] The spectrum of r-GO-Apy (Fig. 2b) shows two characteristic bands that appeared at 228 and 318 nm. The band that appeared at 318 nm is corresponding to the π–π electronic transition of r-GO. In addition, the appearance of a new peak at 228 nm indicates that the Apy group is successfully inserted or complexed by reacting into oxygen functional group present on the r-GO domain through its imine linkage.[38]

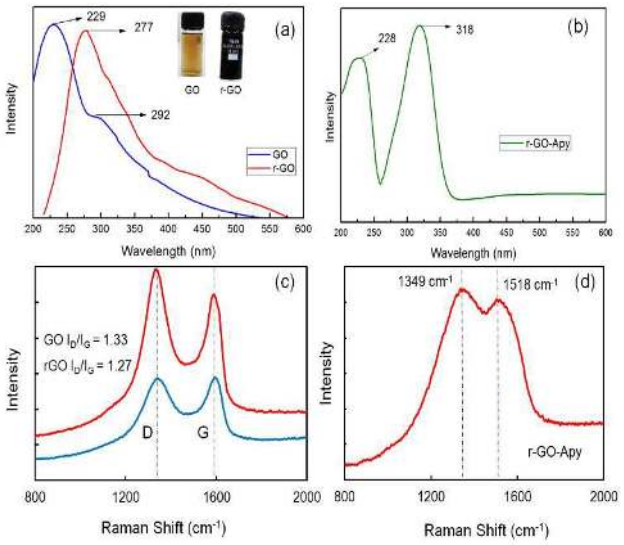

Figure 1:- (a) UV-Vis absorption spectra of GO and r-GO. (b) UV-Vis absorption spectrum of r-GO-Apy. (c) Raman spectra of GO and r-GO. (d) Raman spectrum of r-GO-Apy.

Similarly, Raman spectrum of GO shows an intensive G band at 1600 cm^{-1} and D band at 1342 cm^{-1} which implies the presence of disordered (sp^3) carbon generated by oxidation (Fig. 1c).[12,25,29] Similarly, r-GO exhibited G band at 1599 cm^{-1} along with an intensive D band at 1341 cm^{-1} (Fig. 1c). The ratio of I_D/I_G of GO and r-GO were calculated and found to be 1.33 and 1.27, respectively. The reduction in I_D/I_G ratio of r-GO indicates partial restoration of structural defectiveness after the reduction of GO to the r-GO surface.[28] Raman spectrum of r-GO-Apy hybrid shows that the D and G bands shifted to 1349 cm^{-1} and 1518 cm^{-1}, respectively (Fig. 1d). The shift of D and G bands from 1341 cm^{-1} to 1349 cm^{-1} and from 1599 cm^{-1} to 1518 cm^{-1} for r-GO and r-GO-Apy shows the insertion of Apy in the r-GO domain and this further supported the observation made in UV–Vis absorption spectrum measurements.[34]

HR–TEM analysis was carried out to understand the surface morphology of r-GO and r-GO-Apy. Fig. 2a shows the discontinuous amorphous structure of GO. In Fig. 2b, the well-defined crystalline structure of r-GO sheets clearly specifies the reduction of oxygen functional groups, which was confirmed by the Raman and UV–Vis spectroscopy measurements. Additionally, the magnified version of Fig. 2c exhibits four layers structure of r-GO. Fig. 2d shows the

View Article Online
DOI: 10.1039/C6RA13911F

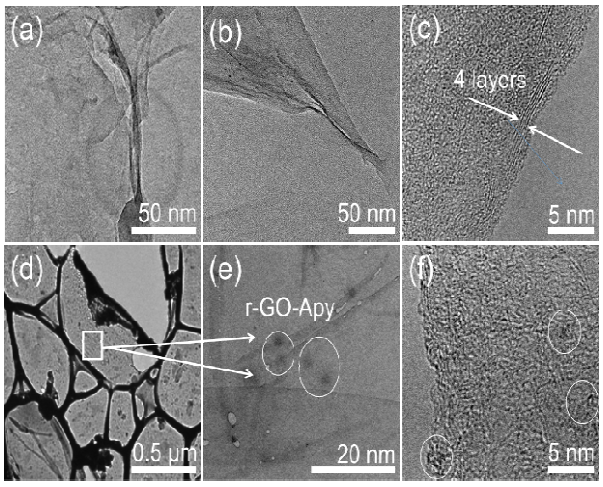

Figure 2:- (a) HR-TEM image of GO. (b) HR-TEM image of r-GO. (c) HR-TEM Higher resolution image of r-GO. (d) HR-TEM image of r-GO-Apy. (e) & (f) Magnified images of r-GO-Apy.

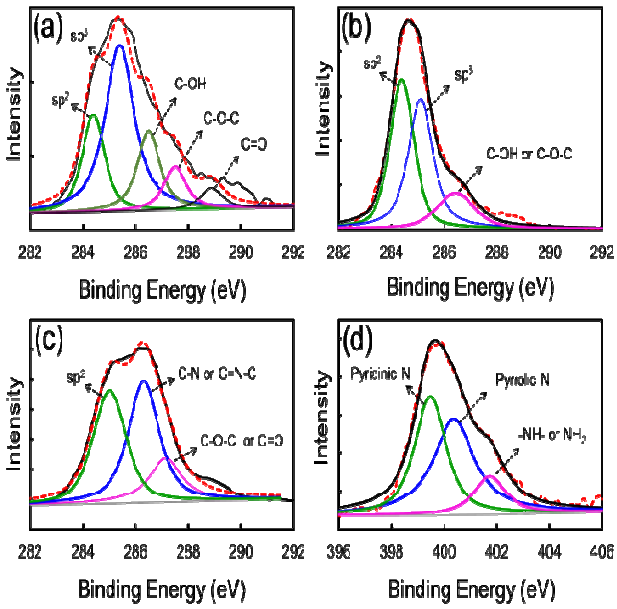

Figure 3:- (a) XPS spectrum of GO in C 1s region. (b) XPS spectrum of r-GO. (c) XPS spectrum of r-GO-Apy in C 1s region. (d) XPS spectrum of r-GO-Apy in N 1s region.

homogeneous distribution of Apy on the r-GO surface. The magnified image of r-GO-Apy in Figure 2e and 2f further confirms the fact that Apy was uniformly anchored on the thin layer of r-GO sheets.

XPS analyses were performed on GO, r-GO and r-GO-Apy to evaluate the effectiveness of reduction, functionalization and chemical composition (C 1s and N 1s). The C 1s core level spectrum of GO nanosheets is shown in Fig. 3a. C 1s region of GO exhibits five well set binding energy configurations, identified as 284.3, 285.1, 286.3, 287.8, and 289 eV for sp^2, sp^3, C-OH (hydroxyl), C-O-C (epoxy), and C=O (carboxy) functional groups, respectively.[28] However, in r-GO the intensity of sp^3 peak at 285.1 eV is found to be reduced and a considerable increase in the sp^2 peak at 284.3 eV implies the effective reduction of hydroxyl and epoxy groups(Fig. 3b).[39] The C 1s region of r-GO-Apy exhibits a well distinct peak at 284.8 eV attributed to sp^2 carbon.[40] The new peak appeared at 286.1 eV corresponds to the insertion of imine (-NH-) group into the r-GO network (Fig. 3c).[17] Similarly, The N 1s region of r-GO-Apy shows a broad peak at 399 eV, that implies pyridinic (-C=N-) nitrogen and a peak at 400.6 eV, which is assigned to pyrrole (–C-NH) groups.[41] Additionally, the binding energy of 401.9 eV corresponds to $-NH_2$ or quaternary NH_3 (Fig. 3d). The above observation clearly validates the reduction and insertion of Apy in the r-GO domain.

Performance of r-GO-Apy-CC electrode in SEMR

Initial experiments were carried out with PCC, r-GO-CC and r-GO-Apy-CC electrodes in SEMR and BES under identical experimental conditions. The r-GO-CC electrode exhibits more or less similar behaviour to the PCC electrode in terms of both bacterial attachment and voltage-current response, probably due to the absence of the active functional groups. Therefore, further studies were carried out with PCC and r-GO-Apy-CC electrodes. In SEMR, r-GO-Apy-CC electrode and PCC were kept as the "sacrificial electrode mode" in a separate reactor and monitored for attached bacterial quantity, the attached extracellular polysaccharides, acetate and the total organic carbon (TOC) concentration, periodically. During the reactor start-up, the initial TOC and acetate concentration values were found to be 500 mg L^{-1} and 750 mg L^{-1}, respectively (Figures 4a and 4b). It was found that the acetate concentration is decreased with respect to time and it reached 112 mg L^{-1} for r-GO-Apy-CC and 187 mg L^{-1} for PCC electrode reactor on the eighth day (Fig. 4b). After the addition of acetate on the eighth day, the acetate concentration was increased to 725 mg L^{-1} for r-GO-Apy-CC and 737 mg L^{-1} for PCC. A similar trend was followed in TOC concentration for both the reactors. The fluctuation in TOC is due to alternating consumption of carbon substrate by bacteria and the external addition of acetate. However, a rise in the TOC concentration was observed on the eighth day and after the twelfth day (Fig. 4a). The increased TOC was observed only when the acetate concentration was at a minimum. Therefore, this could be due to dead suspended bacterial biomass or leaching of carbon from the CC electrode.

As the experiment progressed, the attached bacterial density was observed to be higher in r-GO-Apy-CC electrode than it was in the PCC electrode (Fig. 4c). The maximum attached bacterial density on the r-GO-Apy-CC electrode was observed on the sixth (168 ± 7 CFU cm^{-2}) and the twelfth days (285 ± 18 CFU cm^{-2}). The extracellular polysaccharides in both the reactors followed a similar trend with higher concentration observed in the r-GO-Apy-CC electrode (113.28 mg cm^{-2}) as compared to that of PCC electrode (68.65 mg cm^{-2}) (Fig. 4d).

View Article Online
DOI: 10.1039/C6RA13911F

An overall increasing trend was observed in extracellular polysaccharides, whereas attached bacterial count followed the fluctuating trend of TOC. Bacterial cells reduced in count responding to the decrease in the substrate due to endogenous decay,[42] whereas the extracellular polysaccharide matrix remains unchanged with respect to TOC. Increased extracellular polysaccharides in the system indicate efficient attachment of bacteria to the electrode.[43]

At the end of the experiment, a piece of r-GO-Apy-CC and PCC electrodes were sacrificed for SEM analysis. The SEM images of PCC rendered a small bacterial colonization superficially attached on the electrode surface, while hardly any bacterial cells were present on the interior fibre cloth region (Fig. 4e). On the other hand, r-GO-Apy-CC exhibits a large area of bacterial colonization adhered on the electrode surface (Fig. 4f). This could be due to the following possible reasons. (i) r-GO present in the modified electrode agrees well with the outer cytochromes of the bacterial cells and improves EET efficiency through imine (-NH-) and pyridinic (-N=C-) groups.[2,3,29,32,44,45] (ii) r-GO grafted over the CC provides large specific surface area than does PCC, which results in increased active sites for bacterial colonization.[2,3,11,12,14,15,29,34,45] Moreover, the functionalization of r-GO with Apy increases the porosity of nanostructure, and it leads to dense adhesion of bacterial cells on the electrode surface.[29] (iii) The biocompatibility of r-GO not only improves bacterial adhesion but also promotes the interaction among microbes, substrates and electrodes.[20,23] This assumption is valid in the present study as the rate of acetate degradation is always higher in r-GO-Apy-CC than it is in PCC irrespective of a similar degradation trend. This may be due to the fact that exoelectrogens incorporated r-GO-Apy into their EET pathways through imine (-NH-) and pyridinic (-N=C-).[32]

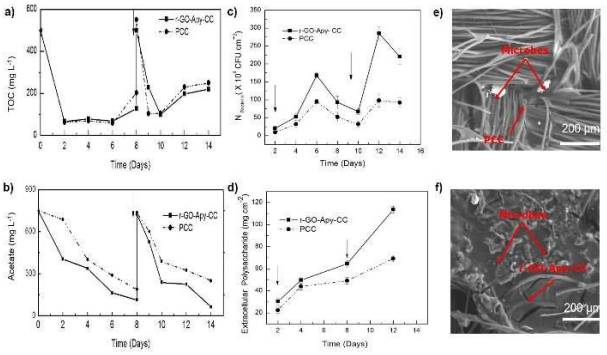

Figure 4:- (a) Temporal variation of total organic carbon concentration (TOC). (b) Temporal variation of acetate concentration (Arrow mark indicates the addition of substrate). (c) The number of bacterial colonies formed on electrode over time. (d) Extracellular polysaccharide content of attached biomass over time. (e) SEM image of PCC after biofilm attachment. (f) SEM image of r-GO-Apy-CC after biofilm formation.

Performance of r-GO-Apy-CC electrode in BES

The electrochemical behaviour of both r-GO-Apy-CC and PCC electrodes were investigated in 1 M NaOH solution with a potential range of –1 V and +1 V versus that of Ag/AgCl. Cyclic voltammetry (CV) analysis of r-GO-Apy-CC exhibited a pair of well-defined redox waves at a scan rate of 100 mV s^{-1} (Fig. 5a). However, the CV of PCC renders almost no peaks with a negligibly low current density response. While comparing with PCC, r-GO-Apy-CC exhibits large CV loop area with significant current density response, which clearly indicates that the coating of r-GO-Apy on PCC remarkably increases its electrochemical performance. Also, the hybrid shows two well-resolved redox peaks due to the presence of pyridinic (-N=C-) groups and imine (-NH-) groups in the r-GO-Apy domain.

BES was employed to study the electrochemical catalytic behaviour of electrode for biofilm formation.[46] During BES operation, CV was monitored with a potential window from 0.6 V to + 0.4 V at 24 h time intervals. The voltamperometric response displayed substantial variations in the electron discharge properties as a function of the electrode material over a period of time (Figures 5b and 5c). Higher redox catalytic current densities were recorded in r-GO-Apy-CC electrode than in PCC throughout the cycle of operation. Initially, the oxidation current density for r-GO-Apy-CC was observed at 0.27 mA cm^{-2}, and the progress in biofilm

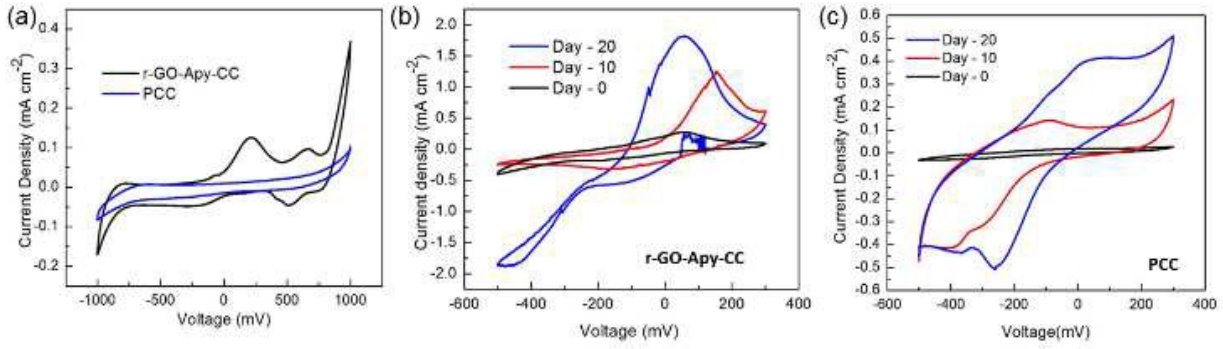

Figure 5:- (a) Electrochemical characterization of r-GO-Apy-CC and PCC electrode by CV in 1M NaOH solution. (b) CV of r-GO-Apy-CC electrode in a BES at a scan rate of 5 mV s^{-1}. (c) CV of PCC electrode in a BES at a scan rate of 5 mV s^{-1}.

View Article Online
DOI: 10.1039/C6RA13911F

formation on the electrode subsequently increased the response of current density to 1.22 mA cm^{-2} and 1.84 mA cm^{-2} during 10 and 20 days, respectively (Fig. 5b). On the other hand, PCC electrode exhibited an oxidative current density of 0.13 mA cm^{-2} and 0.40 mA cm^{-2} after 10 and 20 days of operation, respectively (Fig. 5c). These results critiqued the hypothesis that r-GO-Apy-CC electrode facilitates efficient attachment of biofilm on the electrode and expedites large current density response over a period of time than does PCC.[12,25,38]

Performance of r-GO-Apy-CC electrode in MFC

The performance of r-GO-Apy-CC and PCC for electricity generation was investigated by keeping these as anodes in dual-chambered MFCs. During the start-up period it was observed that, r-GO-Apy-CC exhibits a higher open circuit voltage of 657.5 mV than does PCC (500 mV). The current production from each electrode was monitored by keeping 1000 Ω resistor over a period of time after the acclimatization stage. Both the electrodes exhibited a typical current generation profile in accordance with the addition of acetate, and the results concurred with those obtained in other studies.[2,16,32] An increase in current density was observed continually during the addition of substrate and this maintains a steady state condition for a period of time (Fig. 6a).[2] The modified r-GO-Apy-CC delivered higher current density than did the PCC electrode throughout the experiment, possibly because of the functional group present on the surface. In addition, polarization studies were performed to determine the maximum power generated from the MFC when the device was in the steady state condition. During polarization experiment, MFC device employed with r-GO-Apy-CC shows substantially higher power density (1253 mW m^{-2}; 5.27 A m^{-2}) than does PCC (663.47 mW m^{-2}; 2.65 A m^{-2}) (Fig. 6b). The obtained power density from r-GO-Apy-CC is nearly two times higher than that of the MFC device employed with PCC and the results are comparable with those of the previous studies performed with the graphene – a conductive polymer hybrid material, as compiled in Table 1.

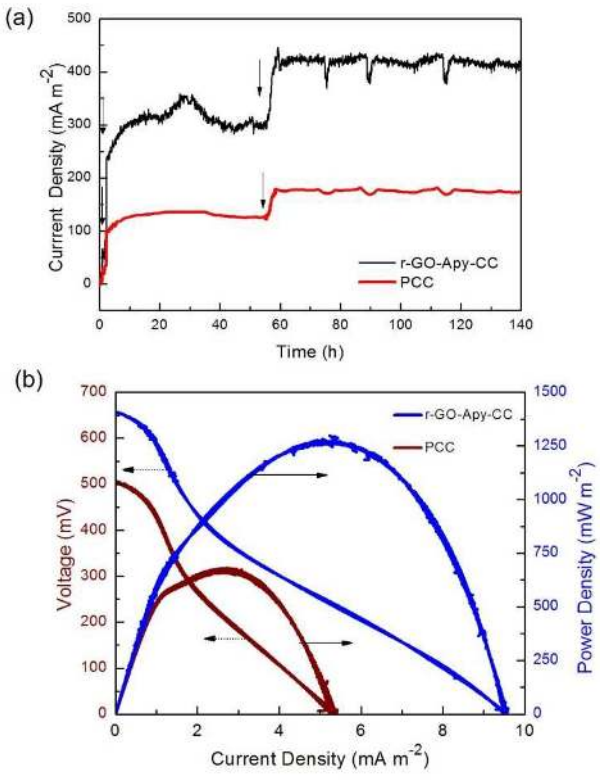

Figure 6:- (a) Current generation over a period of time (Arrow mark indicates the addition of substrate). (b) Power output and polarization.

Table 1. Maximum power density obtained from different anode material.

Hybrid/Composite material	Anode	Power Output (mW m^{-2})	Refere-nce
Aminopyrazine/ reduced graphene oxide	Carbon cloth (2.5 cm X 2.5 cm)	1253	Present study
polypyrrole/ graphene oxide	graphite felt (3 cm×2 cm)	1326	34
Polypyrrole/ reduced graphene oxide	Carbon cloth (1 cm×1.5 cm)	1068	38
polyaniline / reduced graphene oxide	Carbon cloth (1.8 cm×1.8 cm)	1390	12
polyaniline / graphene nanoribbons	Carbon paper (4 cm^2)	856	29
Polyaniline/ 3D graphene	Carbon cloth (2 cm× 4 cm)	768	45
Ionic liquid	Carbon paper	601	32

The schematic view at the interface between r-GO-Apy-CC electrode and bacteria is shown in Fig. 7. The insertion of low organic molecule Apy with r-GO domain increases the distance between the r-GO layers and displays high dispersion in a solvent, which is used for thin layer coating. In this study, UV-Vis, Raman spectrum, and XPS analysis have confirmed an increase in sp^2 carbon on graphene sheets due to the decreased oxygen content, results efficient in π–π conjugation between Apy and graphene sheets lead to an improved electron transfer. The hybridized r-GO-Apy-CC increases the hydrophilicity of the CC, and the imine (-NH-) and pyridinic (-

View Article Online
DOI: 10.1039/C6RA13911F

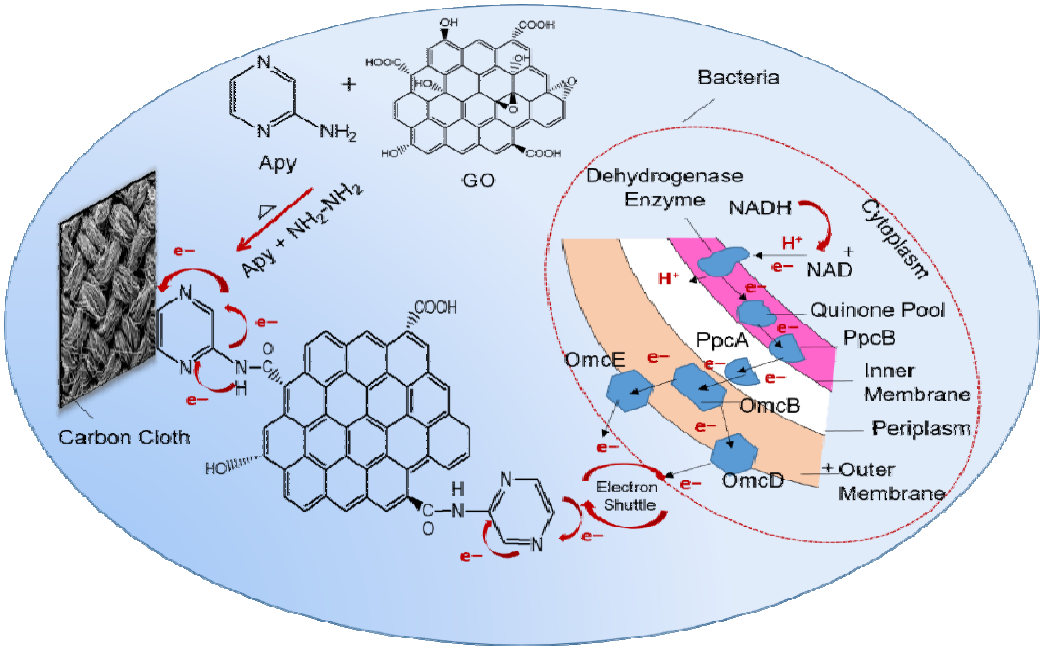

Figure 7:- Schematic view of the interface between r-GO-Apy-CC electrode and bacteria.

N=C-) groups present in the Apy imparts an overall positive charge to the electrode. In fact, the bacterial cells are negatively charged which results in a large area of bacterial colonization due to electrostatic attraction.[13,29] However, most of the commercially available electrode materials are inefficient to interact with the bacterial cells lying very close to the electrode surface due to electrical double-layer mechanism.[11,36] Imine (-NH-) and pyridinic (-N=C-) groups present in the r-GO-Apy-CC electrode material undergo redox mechanism and are protruded to reach the outer cytochrome of the bacterial cells, and transfer electrons to the electrode efficiently (Fig. 7).[20] This could be the reason for a large current density response of r-GO-Apy-CC in BES and MFC reactors than with the reactors employed with PCC. Furthermore, imine (-NH-) and pyridinic (-N=C-) groups present in the r-GO-Apy-CC act as active sites which enhance π–π transitions between the electrode and bacteria. These active sites reduce the activation energy at the electrode biofilm interfaces, which eventually diminishes the electrode double layer thickness formed by two opposite charges.[11,24,34,47] As a result, polarization between electrode and electrolyte will reduce, which ultimately accelerate the adhesion of bacteria on the electrode surface.

Conclusion

In summary, low molecular Apy moieties unified with r-GO was synthesized and fabricated with CC (r-GO-Apy-CC) to form a novel anode material in a two-chambered MFC. UV-VIS, Raman, XPS and TEM results confirmed that Apy was covalently bonded through its imine (-NH-) link to the r-GO, forming highly conductive networks. The result of CV studies performed in BES reactor displays high current density-voltage responses over a period of time which confirms the imine (-NH-) and pyridinic (-N=C-) groups present in the r-GO-Apy-CC which undergoes redox mechanism and facilitates efficient bacterial attachment in the SEMR system. In MFC, r-GO-Apy-CC exhibits substantially higher power density (1253 mW m^{-2}; 5.27 A m^{-2}) which is nearly two times higher than that of the MFC device employed with PCC. This work is an insight to use low molecular organic moieties unified to r-GO as an electrode material, and the advantage of using low molecular organic moieties is that the exoelectrogens can easily incorporate the functional group into their EET pathways under redox mechanism. This study adds new aspects of designing functionalized graphene as an anode in the MFCs as well as in other emerging graphene application.

Experimental Section

Materials and methods

Biofilm growth on modified electrode

Sacrificial electrode mode reactor (SEMR) was fabricated as shown in Fig.8a, to study the efficacious growth of biofilm on the surface of r-GO-Apy-CC (The detailed synthesis procedure of r-GO-Apy-CC, GO and r-GO are given in the electronic supplementary information file). SEMR comprises a high purity quartz glass beaker (500 mL) with an airtight polytetrafluoroethylene (PTFE) cap, mounted over silicon encapsulated PTFE ring. In SEMR, 7 electrodes (each measuring 1 cm × 1 cm) were suspended systematically through copper

View Article Online
DOI: 10.1039/C6RA13911F

wires and each electrode was taken for analysis once in every 48 h interval of time. The reactor was filled with synthetically prepared wastewater autoclaved previously at 121°C for 15 min. The contents of the wastewater were sodium acetate (1 g L^{-1}) as the sole carbon source with macronutrients of NH_4Cl, 125 mg L^{-1}; $NaHCO_3$, 125 mg L^{-1}; $MgSO_4.7H_20$, 51 mg L^{-1}; $CaCl_2.2H_2O$, 300 mg L^{-1}; $FeSO_4.7H_2O$, 6.25 mg L^{-1} and other micronutrients (1.25 mL L^{-1}) were prepared as reported in Lovely and Philips.[48] In addition, nitrogen gas was continuously purged to the wastewater to maintain anaerobicity, and the pH value was brought to 7 by adding H_2SO_4 (0.1 M) and NaOH (0.1 M) solutions. Subsequently, the medium was inoculated by scraping the biofilm off from the anode (50 cm^2) of the previously working MFCs to ensure the occurrence of electrochemically active bacteria.[36] Simultaneously, the electrochemical responses of the bacteria on the electrode were investigated in a separate reactor, namely the BES (Fig.8b). The reactor design and the wastewater composition adopted for BES were exactly the same as SEMR, and CV was performed to monitor current production as a function of potential over a period of time. To compare the efficiency of r-GO-Apy-CC, PCC with the same geometric area was maintained in other two reactors as the control.

MFC construction

The experimental setup used for an MFC is described in the study by Gangadharan and Nambi.[49] A two-chambered reactor of 500 mL capacity was made with plexiglass acrylic tube and separated from each other by a proton exchange membrane (Nafion 117; Sigma-Aldrich). r-GO-Apy-CC (2.5 cm × 2.5 cm) was used as an anode and its performance was compared with that of the PCC (2.5 cm × 2.5 cm). PCC (2.5 cm X 2.5 cm) was used as a cathode throughout the experiment unless stated otherwise. Synthetic wastewater of 300 mL was prepared as explained in the previous section and was used as an anolyte. Potassium dichromate ($K_2Cr_2O_7$; 99%; Sigma-Aldrich) of a concentration of 100 mg L^{-1} was used as the catholyte. $K_2Cr_2O_7$ was chosen as the catholyte owing to its high redox potential (E^0 - 1:33 V at 25°C) which is considerably higher than that of oxygen.[49] The pH value of the catholyte solution was maintained at 7 by adding a phosphate buffer solution (13.60 g L^{-1} of KH_2PO_4 and 2.33 g L^{-1} of NaOH) and the catholyte conductivity was improved by adding 11.70 g L^{-1} of NaCl.

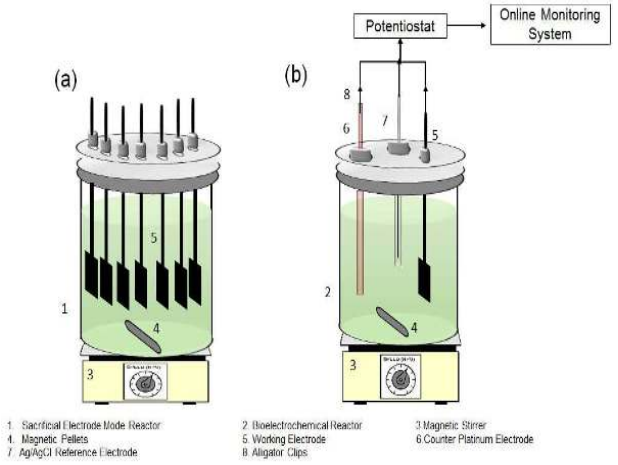

Figure 8:- (a) Sacrificial Electrode Mode Reactor (SEMR). (b) Bioelectrochemical system Reactor.

Measurements and analyses

Chemical Analysis

In SEMR reactor, the substrate degradation was monitored by a decrease in TOC value (TOC-V CPH, Shimadzu). Acetate concentration was analysed by Ion Chromatography (Dionex, USA) using IonPac AS18 anion exchange column. The degradation efficiency was calculated according to Eqn.1.

$$\text{Degradation Efficiency (\%)} = \frac{A-B}{A} \times 100 \qquad (1)$$

Where, A is the initial TOC/ acetate concentration in mg L^{-1} and B is the observed TOC/ acetate concentration in mg L^{-1}.

Biofilm Characterization

The growth of biofilm on electrodes in SEMR was monitored by pour plate method as well as by the extracellular polysaccharide concentration. Every 24 h, the electrodes were carefully removed from the reactor and vigorously shaken with deionized water to ensure the detachment of bacteria and the supernatant was analysed for attached bacterial colony count (CFU cm^{-2}) by the pour plate method.[50] The supernatant with electrode was further centrifuged at 10,000 rpm for 5 min. The concentrated biomass was re-suspended with NaCl buffer (0.85 %) and sonicated for 2 min. After sonication, the mixed supernatant was centrifuged at 10,000 rpm for 2 min and the supernatant solution was further analysed for extracellular polysaccharide concentration by phenol–sulfuric acid method.[43] Scanning Electron Microscopy (SEM; Quanta 200 Philips) was employed to confirm the growth of a biofilm on the electrodes.

Electrochemical Measurements

In BES, CV analysis was performed separately with r-GO-Apy-CC (1 cm × 1 cm) or with PCC as working electrodes, a saturated Ag/AgCl (+ 0.197 V vs. SHE) as a reference electrode and a platinum electrode as a counter electrode (Fig. 8b).[46] In MFC, a multichannel (4-channel) potentiostat (Bio-Logic, India) was employed to study the current production as well as the polarization curve. The BES and MFC were connected to the potentiostat and the data were constantly monitored using the EC lab software. The value of power was calculated by multiplying the measured current with voltage, and the current and power were normalized to the anode surface area (m^2) to obtain current density and power density, respectively. The pH of the anolyte and catholyte was continuously monitored by providing online pH probe system (ADSENSORS Pvt. Ltd., India) in the anode and cathode chambers of the MFC, respectively.

Morphology and structural characterization

The structural morphology of r-GO-Apy hybrid was investigated by high-resolution transmission electron

View Article Online
DOI: 10.1039/C6RA13911F

microscopy (HR-TEM, JEOL JEM 2100F). High-resolution X-ray photoelectron spectroscopy (HR-XPS, PHI Quantera SXM, ULVAC Inc.) was performed to examine the binding energies of carbon, nitrogen and oxygen present in the r-GO-Apy hybrid. An ultraviolet-visible (UV-Vis) spectrometer (Shimadzu, Japan, Model 1800) was employed to study the absorption spectra of GO, r-GO, and r-GO-Apy hybrid. The Raman spectra of GO, r-GO and r-GO-Apy were performed using a Renishaw in via confocal micro-Raman spectrometer using a 633 nm argon laser as the excitation source.

Acknowledgements

The authors gratefully acknowledge the financial support of Department of Science & Technology (DST) [No. SR/WOS-A/ET-1017/2014] and Ministry of Human Resource Development, Government of India in carrying out this research work.

References:

1 B. E. Logan, B. Hamelers, R. Rozendal, U. Schröder, J. Keller, S. Freguia, P. Aelterman, W. Verstraete and K. Rabaey, *Environ. Sci. Technol.*, 2006, 40, 5181–5192.
2 R. Karthikeyan, B. Wang, J. Xuan, J. W. C. Wong, P. K. H. Lee and M. K. H. Leung, *Electrochim. Acta*, 2015, **157**, 314–323.
3 Y. Gao, H. Ryu, J. W. Santo Domingo and H.-S. Lee, *Bioresour. Technol.*, 2014, **153**, 245–53.
4 C. I. Torres, R. Krajmalnik-Brown, P. Parameswaran, A. K. Marcus, G. Wanger, Y. A. Gorby and B. E. Rittmann, *Environ. Sci. Technol.*, 2009, **43**, 9519–9524.
5 C. I. Torres, A. K. Marcus, H.-S. Lee, P. Parameswaran, R. Krajmalnik-Brown and B. E. Rittmann, *FEMS Microbiol. Rev.*, 2010, **34**, 3–17.
6 P. Parameswaran, C. I. Torres, H. S. Lee, R. Krajmalnik-Brown and B. E. Rittmann, *Biotechnol. Bioeng.*, 2009, **103**, 513–523.
7 H.-S. Lee, P. Parameswaran, A. Kato-Marcus, C. I. Torres and B. E. Rittmann, *Water Res.*, 2008, **42**, 1501–10.
8 D. R. Lovley, *Curr. Opin. Biotechnol.*, 2008, **19**, 564–71.
9 J. Wei, P. Liang and X. Huang, *Bioresour. Technol.*, 2011, **102**, 9335–9344.
10 M. Zhou, M. Chi, J. Luo, H. He and T. Jin, *J. Power Sources*, 2011, **196**, 4427–4435.
11 C. Feng, Z. Lv, X. Yang and C. Wei, *Phys. Chem. Chem. Phys.*, 2014, **16**, 10464–72.
12 J. Hou, Z. Liu and P. Zhang, *J. Power Sources*, 2013, **224**, 139–144.
13 S. Cheng and B. E. Logan, *Electrochem. commun.*, 2007, **9**, 492–496.
14 H.-T. Chou, H.-J. Lee, C.-Y. Lee, N.-H. Tai and H.-Y. Chang, *Bioresour. Technol.*, 2014, **169**, 532–536.
15 J. J. Sun, H. Z. Zhao, Q. Z. Yang, J. Song and A. Xue, *Electrochim. Acta*, 2010, **55**, 3041–3047.
16 S. Chen, H. Hou, F. Harnisch, S. a. Patil, A. a. Carmona-Martinez, S. Agarwal, Y. Zhang, S. Sinha-Ray, A. L. Yarin, A. Greiner and U. Schröder, *Energy Environ. Sci.*, 2011, **4**, 1417.
17 H. Wang, G. Wang, Y. Ling, F. Qian, Y. Song, X. Lu, S. Chen, Y. Tong and Y. Li, *Nanoscale*, 2013, **5**, 10283–10290.
18 M. Ghasemi, W. R. W. Daud, S. H. a. Hassan, S.-E. Oh, M. Ismail, M. Rahimnejad and J. M. Jahim, *J. Alloys Compd.*, 2013, **580**, 245–255.
19 Y. Zhu, S. Murali, W. Cai, X. Li, J. W. Suk, J. R. Potts and R. S. Ruoff, *Adv. Mater.*, 2010, **22**, 3906–3924.
20 H. Yuan and Z. He, *Nanoscale*, 2015.
21 R. S. Dreyer, D. R., Park, S., Bielawski, C. W., & Ruoff, *Chem. Soc. Rev.*, 2010, **39**, 228–240.
22 M. J. Allen, V. C. Tung and R. B. Kaner, *Chem. Rev.*, 2010, **110**, 132–145.
23 E. C. Salas, Z. Sun, A. Lüttge and J. M. Tour, *ACS Nano*, 2010, **4**, 4852–4856.
24 G. Wang, F. Qian, C. W. Saltikov, Y. Jiao and Y. Li, *Nano Res.*, 2011, **4**, 563–570.
25 X. Jiang, S. Lou, D. Chen, J. Shen, W. Han, X. Sun, J. Li and L. Wang, *J. Electroanal. Chem.*, 2015, **744**, 95–100.
26 X. Xie, G. Yu, N. Liu, Z. Bao, C. S. Criddle and Y. Cui, *Energy Environ. Sci.*, 2012, **5**, 6862.
27 S. Pei and H. M. Cheng, *Carbon N. Y.*, 2012, 50, 3210–3228.
28 J. Senthilnathan, Y.-F. Liu, K. S. Rao and M. Yoshimura, *Sci. Rep.*, 2014, **4**, 4395.
29 C. Zhao, P. Gai, C. Liu, X. Wang, H. Xu, J. Zhang and J.-J. Zhu, *J. Mater. Chem. A*, 2013, **1**, 12587–12594.
30 M. Jahan, Q. Bao and K. P. Loh, *J. Am. Chem. Soc.*, 2012, **134**, 6707–6713.
31 S. Mu, *Electrochim. Acta*, 2011, **56**, 3764–3772.
32 C. Zhao, Y. Wang, F. Shi, J. Zhang and J.-J. Zhu, *Chem. Commun. Chem. Commun*, 2013, **49**, 6668–6670.
33 M. M. Stylianakis, E. Stratakis, E. Koudoumas, E. Kymakis and S. H. Anastasiadis, *ACS Appl. Mater. Interfaces*, 2012, **4**, 4864–70.
34 Z. Lv, Y. Chen, H. Wei, F. Li, Y. Hu, C. Wei and C. Feng, *Electrochim. Acta*, 2013, **111**, 366–373.
35 B. Liang, Z. Qin, T. Li, Z. Dou, F. Zeng, Y. Cai, M. Zhu and Z. Zhou, *Electrochim. Acta*, 2015, **177**, 335–342.
36 P. Gangadharan, I. M. Nambi and J. Senthilnathan, *Bioresour. Technol.*, 2015, **195**, 96–101.
37 K. A. Darwish, M. Mounir, A. L. EL-Ansary and H. B. Hassib, 1987, **114**, 265–271.
38 G. Gnana Kumar, C. J. Kirubaharan, S. Udhayakumar, K. Ramachandran, C. Karthikeyan, R. Renganathan and K. S. Nahm, *ACS Sustain. Chem. Eng.*, 2014, **2**, 2283–2290.
39 N. A. Kumar, H.-J. Choi, Y. R. Shin, D. W. Chang, L. Dai and J.-B. Baek, *ACS Nano*, 2012, **25**, 1715–1723.
40 V. Chandra and K. S. Kim, *Chem. Commun. (Camb).*, 2011, **47**, 3942–3944.
41 X. Z. Tang, W. Li, Z. Z. Yu, M. a. Rafiee, J. Rafiee, F. Yavari and N. Koratkar, *Carbon N. Y.*, 2011, **49**, 1258–1265.
42 C. I. Torres, A. K. Marcus and B. E. Rittmann, *Appl. Microbiol. Biotechnol.*, 2007, **77**, 689–97.
43 L. Zhang, X. Zhu, J. Li, Q. Liao and D. Ye, *J. Power Sources*, 2011, **196**, 6029–6035.
44 Y.-X. Huang, X.-W. Liu, J.-F. Xie, G.-P. Sheng, G.-Y. Wang, Y.-Y. Zhang, A.-W. Xu and H.-Q. Yu, *Chem. Commun. (Camb).*, 2011, **47**, 5795–5797.
45 Y. C. Yong, X. C. Dong, M. B. Chan-Park, H. Song and P. Chen, *ACS Nano*, 2012, **6**, 2394–2400.
46 K. Fricke, F. Harnisch and U. Schröder, *Energy Environ. Sci.*, 2008, **1**, 144.
47 Y. Zou, C. Xiang, L. Yang, L.-X. Sun, F. Xu and Z. Cao, *Int. J. Hydrogen Energy*, 2008, **33**, 4856–4862.
48 D. R. Lovley and E. J. Phillips, *Appl. Environ. Microbiol.*, 1988, **54**, 1472–80.
49 P. Gangadharan and I. M. Nambi, *Water Sci. Technol.*, 2015, **71**, 353.
50 H. J. Hoben and P. Somasegaran, *Appl. Environ. Microbiol.*, 1982, 44, 1246–1247.

View Article Online
DOI: 10.1039/C6RA13911F

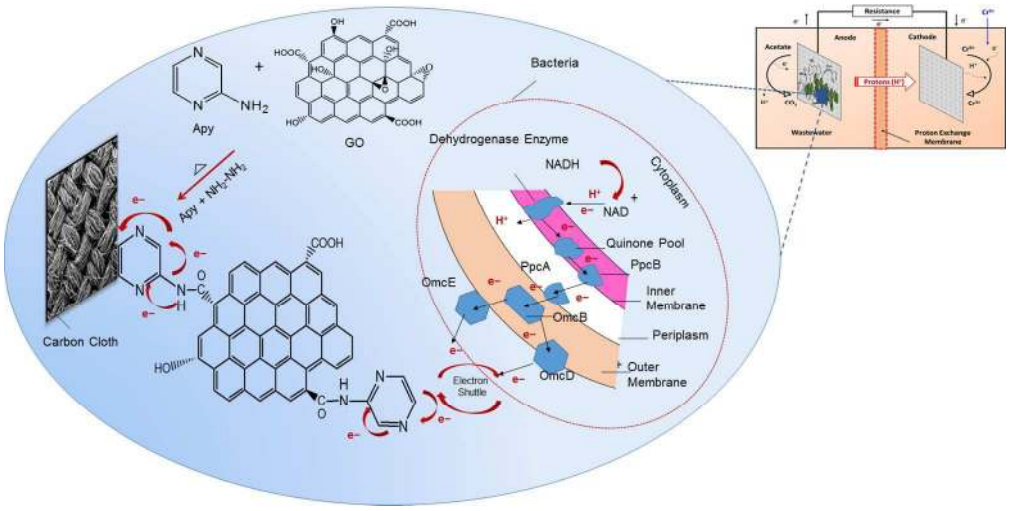

Graphical Abstract

290x145mm (144 x 144 DPI)